Atomistic modelling of $BaTiO_3$ based on first-principles calculations

1999 J. Phys.: Condens. Matter 11 9679

(http://iopscience.iop.org/0953-8984/11/48/325)

J. Phys.: Condens. Matter **11** (1999) 9679–9690. Printed in the UK PII: S0953-8984(99)04090-4

Atomistic modelling of $BaTiO_3$ based on first-principles calculations

S Tinte†, M G Stachiotti†, M Sepliarsky†, R L Migoni† and C O Rodriguez‡

† Instituto de Física Rosario, Universidad Nacional de Rosario, 27 de Febrero 210 Bis, 2000 Rosario, Argentina

‡ IFLYSIB, Grupo de Física del Sólido, CC 565, 1900 La Plata, Argentina

Received 7 May 1999, in final form 21 September 1999

Abstract. Interatomic potentials are determined in the framework of a shell model used to simulate the structural instabilities, dynamical properties, and phase transition sequence of $BaTiO_3$. The model is developed from first-principles calculations by mapping the potential energy surface for various ferroelectric distortions. The parameters are obtained by performing a fit of interatomic potentials to this energy surface. Several zero-temperature properties of $BaTiO_3$, which are of central importance, are correctly simulated in the framework of our model. The phase diagram as a function of temperature is obtained through constant-pressure molecular dynamics simulations, showing that the non-trivial phase transition sequence of $BaTiO_3$ is correctly reproduced. The lattice parameters and expansion coefficients for the different phases are in good agreement with experimental data, while the theoretically determined transition temperatures tend to be too small.

1. Introduction

Despite sharing a common formula ABO_3 and a high-temperature cubic phase, the ferroelectric and related perovskites exhibit a variety of structural phase transitions. The ideal cubic structure displays a wide variety of energy instabilities. These may involve rotation and distortions of the oxygen octahedra as well as displacement of the cations from their ideal sites.

Among the ferroelectric perovskites, $BaTiO_3$ has been one of the most exhaustively studied materials. At high temperatures, it has the classic perovskite structure. This is cubic centrosymmetric, with the Ba at the corners, Ti at the centre, and oxygens at the face centres. However, as the temperature is lowered, it goes through a succession of ferroelectric phases with spontaneous polarizations along the [001], [011], and [111] directions of the cubic cell. These polarizations arise from net displacements of the cations with respect to the oxygen octahedra along the above directions. Each ferroelectric phase involves also a small homogeneous deformation which can be thought of as an elongation of the cubic unit cell along the corresponding polarization direction. Thus the system becomes tetragonal at 393 K, orthorhombic at 278 K, and rhombohedral below 183 K.

First-principles calculations have contributed greatly to the understanding of the origins of these structural phase transitions, providing considerable insight into the nature of the ferroelectric instabilities. These methods are based upon a full solution for the quantum mechanical ground state of the electron system within the local density approximation (LDA) to density functional theory (DFT). The calculations for $BaTiO_3$ indicate that the ferroelectric instability arises from a delicate cancellation between short-range repulsive and ionic forces, demonstrating that the hybridization between the titanium 3d states and the oxygen 2p states

0953-8984/99/489679+12$30.00

is essential for ferroelectricity [1, 2]. This hybridization is also responsible for the giant values of the Born effective charges in ABO_3 perovskites [3–6].

The two more widely used approximations to DFT, LDA and GGA (generalized gradient approximation), underestimate and overestimate the equilibrium volume of ferroelectric perovskites [7, 8]. As a result, quantities that depend sensitively on the lattice constant, such as ferroelectric instabilities, are seriously affected when they are evaluated at the theoretical equilibrium volume. On the other hand, the results are closer to the experimental behaviour if one works at the experimental lattice constants.

Although first-principles methods are extremely precise, they are restricted to studying zero-temperature properties. For the study of the thermal behaviour of perovskites, a very successful approach has been developed on the grounds of effective Hamiltonians. In this approach, a model Hamiltonian is written as a function of a reduced number of degrees of freedom (a local soft-mode amplitude vector and a local strain tensor), and the Hamiltonian parameters are determined in order to reproduce the spectrum of low-energy excitations of a given material as obtained from first-principles calculations. This approach has been applied with considerable success to several ferroelectric materials, including $BaTiO_3$ [9].

Atomistic simulation methods are well known to play an important role in solid-state and material sciences. The traditional approach consists in adjusting unknown model parameters to macroscopic crystal properties. The success and scope of the field is evident from the large number of investigations on complex oxides crystals. In this way, Lewis and Catlow [10] developed a shell model fitted for $BaTiO_3$ to reproduce its lattice spacing, elastic properties, and dielectric constants. This model has been applied recently to the study of point defects [11] and surface structure [12].

Regarding dynamical properties, the most successful approach to the lattice dynamics study of ferroelectric perovskites has been carried out in the framework of the non-linear oxygen polarizability model [13]. In this shell model, an anisotropic core–shell interaction is considered at the O^{2-} ions, with an harmonic core–shell interaction on the O–A planes, and a fourth-order core–shell interaction along the O–B bond. The model parameters were obtained by fitting experimental phonon dispersion curves, and the soft-mode temperature dependence was studied within the self-consistent phonon approximation. This model has been applied to several ferroelectric perovskites [14–17], including $BaTiO_3$ [18].

Although both above-mentioned shell models fitted for $BaTiO_3$ reproduce several properties of its cubic phase, they do not describe its structural instabilities and phase transition sequence. Nowadays it is possible to perform first-principles calculations on complex phases, and more reliable potentials can be derived. However, obtaining accurate interatomic potentials which are able to describe the structural instabilities of ABO_3 perovskites constitutes a challenging problem.

The goal of this work is to obtain an atomistic model for $BaTiO_3$ which describes accurately its dynamical properties, energy instabilities, and phase transition sequence. To this end, we develop a shell model from first-principles calculations by mapping the potential energy surface for various configurations of some carefully selected atomic displacements. The potential parameters are obtained by performing a fit of interatomic potentials to this energy surface. The temperature-driven structural transitions are then investigated through molecular dynamics simulations.

2. Model and computational details

For the atomistic simulation we chose the non-linear oxygen polarizability model previously applied to $BaTiO_3$ [18], since this model provided an accurate description of its lattice

dynamics. Here each ion is modelled as a massive core linked to a massless shell. An anisotropic core–shell interaction is considered at the O^{2-} ions, with a fourth-order core–shell interaction along the O–Ti bond. This emphasizes the large anisotropic polarization effects at the oxygens produced by variations of the O–B distance [16]. Such effects are expected in view of the strong environment-dependent oxygen polarizability and its enhancement through hybridization between oxygen p and transition metal d orbitals. The Ba and Ti ions are considered isotropically polarizable.

The first-principles total-energy calculations were performed within the LDA to DFT, using the highly precise full-potential linear augmented-plane-wave (LAPW) method. We use the WIEN97 implementation of the method [19] which allows the inclusion of local orbitals (LO) in the basis, making possible a consistent treatment of semicore and valence states in one energy window, hence ensuring proper orthogonality. The Ceperley and Alder [20] exchange–correlation potential for the many-body interactions between electrons, as parametrized by Perdew and Zunger [21], was used.

Muffin-tin sphere radii $(R_i) = 2.0$, 1.95 and 1.50 au were used for Ba, Ti and O, respectively. The value of the parameter RK_{max}, which controls the size of the basis sets in these calculations, was chosen to be 8. This gives well converged basis sets consisting of approximately 1100 LAPW functions plus local orbitals.

We introduced LO to include the following orbitals in the basis set: Ba 5s, 5p and 4d; Ti 3s and 3p; and O 2s. Integrations in reciprocal space were performed using the special-points method. We used $6 \times 6 \times 6$ meshes which represent 250 k-points in the first Brillouin zone. Convergence tests indicate that only small changes result from increasing to a denser k-mesh.

In order to better quantify the ferroelectric instabilities of the cubic phase, we determined the phonon frequencies and polarizations of the infrared-active Γ_{15} modes, which include the 'ferroelectric soft' mode, by calculating atomic forces for several small displacements ($\sim$0.01 Å) consistent with the symmetry of the mode. From the force as a function of displacement, the dynamical matrix was constructed and diagonalized. Finally, the total energy is evaluated as a function of the ferroelectric soft-mode displacement pattern for different directions in the cubic phase. We analyse also the effects of the tetragonal strain by performing the [001] soft-mode displacements at a lattice parameter ratio $c/a = 1.01$ with the same primitive-cell volume.

The shell-model parameters were initially taken from set II in reference [18]. For a numerical simulation of the system across its different phases it is necessary to replace the harmonic force constants (HFC) of the model by pairwise interatomic potentials. Since the HFC for the pairs Ti–O and Ba–O correspond to repulsive interaction, we choose for these the Born–Mayer form $V(r) = ae^{(-r/\rho)}$, which is usual for ionic crystals. For the pair O–O, however, the HFC correspond to an attractive interaction, a fact which is commonly observed in oxides. Therefore we consider in this case a Buckingham potential, $V(r) = ae^{(-r/\rho)} - c/r^6$. The Born–Mayer potential parameters a and ρ for the Ti–O and Ba–O interactions were determined from the corresponding transverse and longitudinal HFC. In the case of the O–O interaction, we need to fix one of the Buckingham parameters to obtain the other two from the HFC. Thus we select an initial value of c which leads to reasonable values of the parameters a and ρ.

Then the potential energy of the model was evaluated for the same displacement patterns as were employed in the *ab initio* total-energy calculations. For each given core configuration the shell coordinates were obtained by solving the adiabatic condition iteratively by a steepest-descent procedure. The results obtained with the initial model parameter set showed serious discrepancies with the *ab initio* results; in particular, the sequence of energy minima in [001], [011] and [111] directions was not in the same order. Thus we modified some model parameters

in order to fit the model energy behaviour to the *ab initio* results. While doing this, we also took care to ensure that the equilibrium lattice constant of the model in the cubic phase reproduces the extrapolation to 0 K of the experimental lattice constant in the cubic phase, which yields $a = 3.995$ Å [22]

It is important to remark that one cannot afford to reproduce 'spot-on' the *ab initio* total-energy surface with such simple interatomic potentials. In addition, the adjustment of the potentials is not a straightforward and easy procedure, because all pair potentials and core–shell coupling constants contribute to the total energy of a given distorted lattice structure. So, the goal was to obtain a model which reproduces, as closely as possible, the energetics and instabilities calculated by the LAPW method.

3. Results

By modifying the potential parameters initially determined, we obtain the energy behaviour shown in figure 1 for various structural distortions. The calculations were performed at the experimental primitive-cell volume for 0 K, which corresponds to a cubic lattice constant $a = 4.003$ Å [23]. The results obtained using the model are compared with the LAPW calculations for the amplitudes of (001), (011), and (111) ferroelectric mode normal coordinates, which are obtained from the following LDA eigenvectors: $e_{\mathrm{Ba}} = -0.017, e_{\mathrm{Ti}} = -0.660, e_{\mathrm{O}_z} = 0.644, e_{\mathrm{O}_y} = e_{\mathrm{O}_x} = 0.273$. For the sake of simplicity, these are represented on the abscissa of the figure through the Ti displacement relative to Ba. A satisfactory overall agreement is achieved. The model yields clear ferroelectric instabilities with similar energetics and minima locations to the LAPW calculation. Energy lowerings of ≈1.2, 1.65 and 1.9 mRyd/cell are obtained for the (001), (011), and (111) ferroelectric mode displacements, respectively; this is consistent with the experimentally observed phase transition sequence. Concerning the energetics for the (001) displacements, it can be also seen in figure 1 that the effect of the

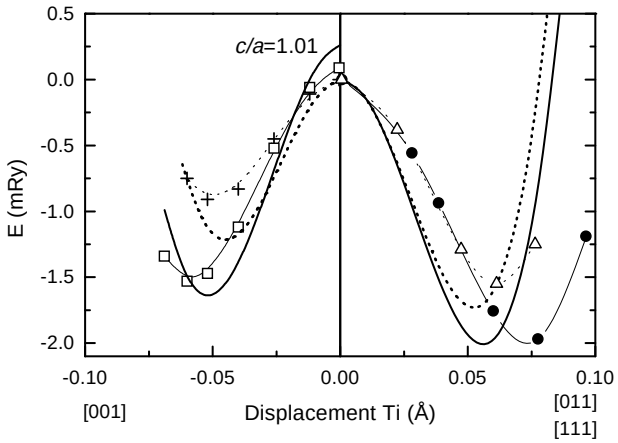

Figure 1. Total energy as a function of the ferroelectric mode displacements along the [001] (left panel), [011], and [111] (right panel) directions. Energies for [001] displacements in a tetragonal strained structure are plotted in the left panel. The ferroelectric normal coordinate is represented through the Ti-relative-to-Ba ionic shifts. The energies are referred to the cubic structure. The results of the LAPW calculation are denoted by the various symbols (+, •, △, □) in both panels. In the left panel, full (broken) lines correspond to the strained (unstrained) structure. In the right panel, full (broken) lines correspond to the [111] ([011]) direction.

tetragonal strain is to stabilize these displacements with a deeper minimum and a higher energy barrier at the centrosymmetric positions. A similar feature is observed for the orthorhombic strain, while an almost negligible effect on the total energies for the rhombohedral strain is observed. The resulting model potential parameters obtained by the fitting procedure are listed in table 1. We remark that the most significant changes were performed in the Ti–O interaction and the core–shell couplings at the oxygen ion, while only slight modifications were introduced in the Ba–O and O–O potential parameters.

Table 1. Potential parameters of the shell model. a, ρ, c: Buckingham parameters; Z, Y: ionic and shell charges; K_2, K_4: on-site core–shell force constants. The symbols $\parallel$ and $\perp$ refer to directions parallel and perpendicular to the Ti–O bond, respectively.

Interaction	a (eV)	ρ (Å)	c (eV Å^{-6})	Ion	Z ($\|e\|$)	Y ($\|e\|$)	K_2 (eV Å^{-2})	K_4 (eV Å^{-4})
Ba–O	864.536	0.38729	0.0	Ba	1.86	−3.76	251	
Ti–O	4526.635	0.25239	0.0	Ti	3.18	−1.58	321	
O–O	4102.743	0.29581	300.0	O	−1.68	−2.59	31.00 $\parallel$ 101.27 $\perp$	3000.00 $\parallel$

The bulk modulus, as in *ab initio* calculations, can be obtained from the evaluation of the total energy as a function of the uniform volume expansion for the cubic phase. The model calculations yield a lattice parameter of 3.99 Å for the static cubic structure. The bulk modulus evaluated at this equilibrium volume is 226 GPa, which agrees fairly well with the LDA value of 195 GPa [8]. The detailed behaviour of the energy as a function of the cubic lattice parameter a is shown in figure 2, where the model's results are compared with LDA calculations. In order to better compare the results, the energy is plotted as a function of $a - a_{eq}$, where a_{eq} is the

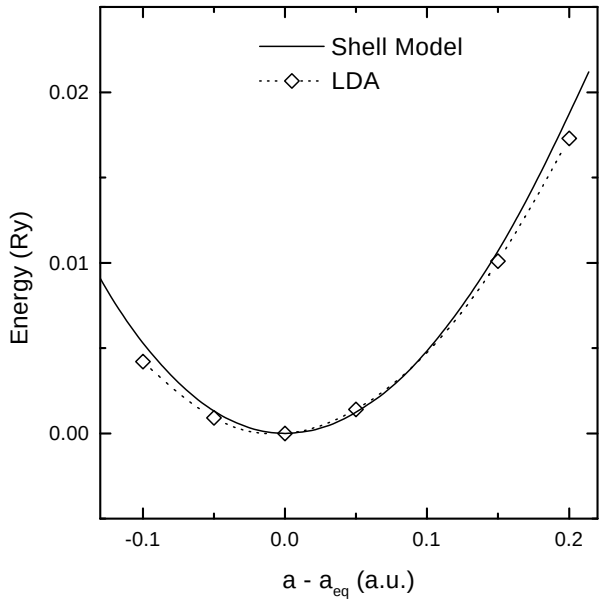

Figure 2. Total energy as a function of the lattice parameter a for cubic $BaTiO_3$. In order to better compare the results, the energy is plotted as a function of $a - a_{eq}$, where a_{eq} is the equilibrium lattice parameter obtained within each approach: 3.99 Å for the shell model, and 3.94Å for the LDA calculations.

equilibrium lattice parameter obtained within each approach: 3.99 Å for the shell model, and 3.94 Å for the LDA calculations. The agreement is again very satisfactory.

Another interesting test of the resulting model concerns its phonon dispersion relations. A first-principles linear response calculation of the phonon dispersion curves of cubic $BaTiO_3$, using the plane-wave pseudopotential approach, revealed the presence of structural instabilities with pronounced two-dimensional character in the Brillouin zone, corresponding to chains of displaced Ti ions oriented along the [001] directions [24]. The same wave-vector dependence of the instabilities had been previously found in $KNbO_3$ through a linear response approach based on a LAPW calculation [25]. To check whether our model is able to reproduce such kinds of instability, we compute the phonon dispersion curves of the cubic structure at the same lattice constant as was used in the previous work [24], i.e. the experimental value $a = 4.00$ Å. The result is shown in figure 3. An excellent agreement with the *ab initio* linear response calculation is achieved, particularly for the unstable phonon modes (compare with figure 2 of reference [24]). Two transverse optic modes are unstable at the Γ point, and they remain unstable along the Γ–X direction with very little dispersion. One of them stabilizes along the Γ–M and X–M directions; and both become stable along the Γ–R and R–M lines. These features, which were also observed in $KNbO_3$, indicate chain-like instabilities in real space. As was already pointed out by Yu and Krakauer [25], the finite thickness of the slab region of instability corresponds to a minimum correlation length of the displacement required to observe an unstable phonon mode. From the phonon dispersion curves showed in figure 3, the length of the shortest unstable chain can be estimated to be $\approx 4\,a$, which is in agreement with the estimation made in reference [24].

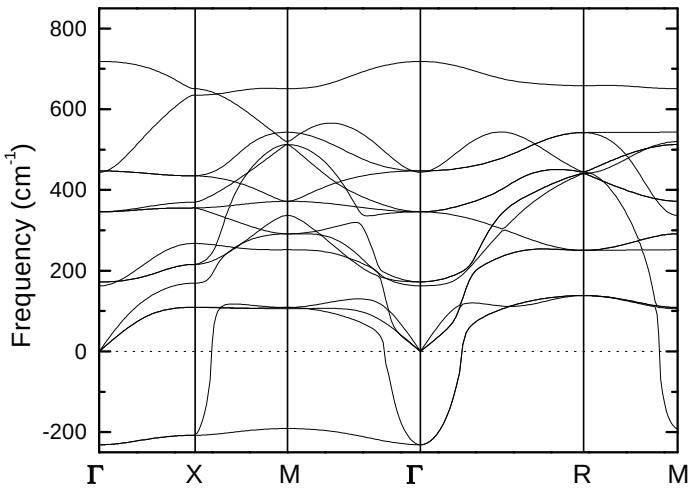

Figure 3. Phonon dispersion curves of $BaTiO_3$ calculated with the optimized model for the cubic structure at the experimental lattice constant. Imaginary phonon frequencies are represented as negative values.

The Γ phonon frequencies obtained from our model have also been compared with LDA and experimental results. It can be observed in table 2 that they are in fairly good agreement. It is worth mentioning also that the eigenvector of the unstable ferroelectric mode as obtained from the model is given by: $e_{\mathrm{Ba}} = -0.009$, $e_{\mathrm{Ti}} = -0.686$, $e_{\mathrm{O}_z} = 0.621$, $e_{\mathrm{O}_y} = e_{\mathrm{O}_x} = 0.269$, which is in very good agreement with the previously given one, obtained from the LAPW calculation.

Table 2. Comparison of the shell-model IR-active optical phonon frequencies (cm^{-1}) with *ab initio* and experimental results.

Mode	Shell model	First principles	Experiment[a]
TO1	231i	219i[b], 239i[c]	Soft
LO1	718	631[b]	717
TO2	172	166[b], 163[c]	181
LO2	162	159[b]	180
TO3	447	453[b], 454[c]	487
LO3	443	445[b]	468

[a] Experimental values from reference [26].
[b] LDA calculation from reference [24].
[c] LDA calculation (present work).

The Born effective charge tensor is conventionally defined as the coefficient of proportionality between the components of the dipole moment per unit cell and the components of the κ-sublattice displacement which gives rise to such a dipole moment:

$$Z^*_{\kappa,\alpha\beta} = \frac{\partial P_\beta}{\partial \delta_{\kappa,\alpha}}. \tag{1}$$

For the cubic structure of ABO_3 perovskites, this tensor is fully characterized by four independent numbers. Experimental data [27] had suggested that the amplitude of the Born effective charges should deviate substantially from the nominal static charges, with two essential features: the oxygen charge tensor is highly anisotropic, and the Ti and $O_\parallel$ effective charges are anomalously large. This was confirmed by more recent first-principles calculations [3–5], demonstrating the crucial role played by the B(d)–O(2p) hybridization as a dominant mechanism for such anomalous contributions [6]. Although our model does not explicitly include charge transfer between atoms, it takes into account the contribution of the electronic polarizability effects through the shell coordinates. So, it is possible to evaluate the Born effective charge tensor calculating the total dipole moment per unit cell created by the displacement of a given sublattice of atoms as a sum of two contributions:

$$P_\alpha = Z_\kappa \delta_{\kappa,\alpha} + \sum_{\kappa'} Y_\kappa w_{\kappa,\alpha}. \tag{2}$$

The first one is the sublattice displacement contribution while the second one is the electronic polarizability contribution. For small displacements, the shell displacements can be readily evaluated in the harmonic approximation, thus leading to an expression for $Z^*_{\kappa,\alpha\beta}$ [28]. The calculated Born effective charges for cubic $BaTiO_3$ are listed in table 3 together with results obtained within different approaches. The two essential features of the Born effective charge tensor of $BaTiO_3$ are satisfactorily simulated in the framework of our model.

So far we have shown that our model for $BaTiO_3$ reproduces several zero-temperature properties which are relevant for this material. To investigate whether the model will prove successful for describing the temperature-driven structural transitions of $BaTiO_3$, we perform constant-pressure molecular dynamics (MD) simulations. Shell-model molecular dynamics, in spite of its long history, is difficult to use due to the treatment of the adiabatic degree of freedoms, i.e. the shells. Most workers have used a steepest-descent method to relax the shell positions iteratively to zero-force positions on each step of the molecular dynamics. Although this procedure has been improved on the basis of conjugate gradient relaxation of the shells [29], in a typical simulation run an average of ten line searches are made within every time step of the simulation, reducing greatly the efficiency of the method in comparison with rigid-ion-model MD simulations. An alternative approach has been introduced by Mitchell

Table 3. Born effective charges of $BaTiO_3$ in the cubic structure.

	Z^*_{Ba}	Z^*_{Ti}	$Z^*_{O_\perp}$	$Z^*_{O_\parallel}$	Reference
Nominal	+ 2	+ 4	−2	−2	
Experiment	+ 2.9	+ 6.7	−2.4	−4.8	[27]
First principles	+ 2.75	+ 7.16	−2.11	−5.69	[5]
	+ 2.70	+ 7.10	−2.12	−5.56	[4]
Shell model (static)	+ 1.86	+ 3.18	−1.68	−1.68	Present work
Shell model (dynamic)	+ 1.93	+ 6.45	−2.3	−3.79	Present work

and Fincham [30] by assigning a small mass to the shells. Thus, their motion, like those of the cores, is found by numerical integration of their equations of motion. They showed that the results of this method are independent of the shell mass, provided that it is small enough, and in agreement with those obtained using relaxation of massless shells. Regarding the efficiency of the method, the shortcoming of this approach is that the time step of the simulation must be reduced in order to provide enough accuracy for the integration of the shell coordinates.

We applied the latter approach in the present MD simulation, which is carried out using the DL-POLY package†. The runs were performed employing a Hoover constant–$(\bar{\sigma}, T)$ algorithm with external stress set to zero; all cell lengths and cell angles were allowed to fluctuate. Periodic boundary conditions over $7 \times 7 \times 7$ primitive cells were considered; the basic molecular dynamics cell therefore contained 1715 ions (plus 1715 shells which are additional degrees of freedom). The time step was 0.4 fs, which provided enough accuracy for the integration of the shell coordinates. The total time of each simulation, after 2 ps of thermalization, was 20 ps.

In figure 4 (top panel) we plot the order parameters (the three components of the mean polarization) as a function of temperature. The cell lattice constants are displayed in figure 4 (bottom panel). At high temperatures, the averaged polarizations p_x, p_y, and p_z are all very close to zero and the three lattice constants have almost identical values. As the system is cooled down below 190 K, p_x acquires a value clearly different from zero, while $p_y \simeq p_z \simeq 0$, and the structure presents a considerable tetragonal strain (see figure 4 (bottom panel)). This indicates the transition from the paraelectric cubic to the ferroelectric tetragonal phase. When the temperature is further reduced, the two lower ferroelectric phases appear: the orthorhombic one below ∼120 K, with clearly finite $p_x \simeq p_y$ and still $p_z \simeq 0$, and finally the rhombohedral phase below ∼90 K, with approximately equal values of the three polarization components.

The structural parameters and spontaneous polarizations, for the different phases of $BaTiO_3$, obtained by the MD simulations are compared with the experimental results in table 4. An excellent overall agreement is obtained, showing that our model reproduces the delicate structural changes involved in the transitions. On the other hand, the theoretically determined transition temperatures tend to be too small compared with experiment. The orthorhombic and tetragonal phases are stabilized over temperature ranges of only ≈30 K and ≈70 K, respectively. Similar features are obtained with the effective Hamiltonian approach [9]. The remarkable point, however, is that the non-trivial phase transition sequence of $BaTiO_3$ is correctly reproduced.

† DL-POLY is a package of molecular simulation routines written by W Smith and T R Forester, Daresbury and Rutherford Appleton Laboratory, Daresbury, UK.

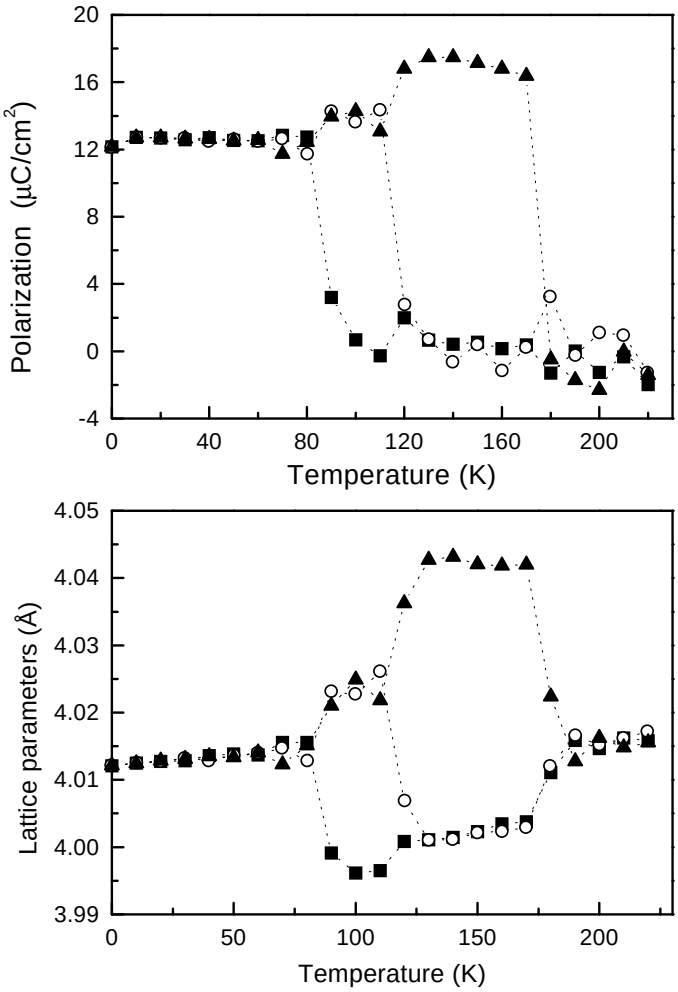

Figure 4. The phase diagram of $BaTiO_3$ resulting from the MD simulation. Top panel: the three components of the average polarization (each one represented with a different symbol); and bottom panel: the corresponding cell parameters (again, each one represented with a different symbol) as functions of temperature.

Since ferroelectricity is very sensitive to volume, the neglect of thermal expansivity in the effective Hamiltonian models could be thought to be responsible for the shifts in the predicted transition temperatures relative to experiment. Our model, however, takes into account the anharmonic interactions among all phonon modes which are responsible for thermal expansion, and, nevertheless, a similar behaviour is obtained for the transition temperatures. This seems to indicate that LDA methods underestimate the ferroelectric instabilities of $BaTiO_3$.

In order to verify that the thermal expansion is properly described by our model, we study the behaviour of the pseudocubic lattice parameter $a = V^{-1/3}$, where V is the cell volume, as a function of temperature. From these data we obtain the expansion coefficients for the different phases listed in table 4. The agreement with the experimental values is quite satisfactory. In order to make a detailed comparison of the thermal expansivity with experimental data [32], we need to rescale the theoretical transition temperatures, since they do not agree with the

Table 4. Structural parameters, cube-edge components of spontaneous polarization, and expansion coefficients for the different phases of $BaTiO_3$. For the orthorhombic phase, the equivalent pseudomonoclinic cell parameters are reported.

Parameter	MD simulation	Experiments
Rhombohedral		
a (Å)	4.012	4.003[a]
α (deg)	89.81	89.84[a]
P (μC cm^{-2})	12.5	13[b]–19[c]
α (10^{-6} °C^{-1})	7.2	5.2[d]
Orthorhombic		
a (Å)	3.995	3.987[a]
$b = c$ (Å)	4.022	4.018[a]
P (μC cm^{-2})	14	14[b]–25[c]
α (10^{-6} °C^{-1})	4.3	4.6[d]
Tetragonal		
a (Å)	4.002	3.999[a]
c (Å)	4.043	4.036[a]
P (μC cm^{-2})	17	17[b]–27[c]
α (10^{-6} °C^{-1})	7.7	6.5[d]
Cubic		
a (Å)	4.016	4.012[e]
α (10^{-6} °C^{-1})	8.5	9.8[d]

[a] Neutron diffraction data from reference [23].
[b] Calculated from the atomic positions, reference [23].
[c] Direct polarization measurements from reference [32].
[d] Dilatometric measurements from reference [33].
[e] From reference [22].

experimental ones. We therefore linearly rescale the theoretical temperatures such that the end points of the stability range of each phase coincide with the experimental T_cs. In addition, in order to ensure that the graph preserves the expansion coefficients obtained, i.e. the slope within each phase, we perform the same rescaling of the ordinate values. In figure 5 we plot $(a - a_0)/a_0$ versus T for both the theoretical and experimental results, where a_0 is the value of a at 0 K. It is interesting to note the volume anomalies at the phase transitions resulting from the model simulation, a feature also observed experimentally, which indicate that the transitions are all first order. In particular, the remarkable volume expansion at the Curie transition is in very good agreement with the dilatometric measurements carried out on polycrystalline samples [32]. According to these investigations, a small volume contraction is found for the lowest transition, while a small volume expansion results from the model simulation. However, one cannot be confident that this is a precise result due to the small temperature range of stability of the orthorhombic phase in our simulation.

In conclusion, we have developed an atomistic model for $BaTiO_3$ which describes its structural instabilities, phonon dispersion curves, and dynamical effective charges in satisfactory agreement with LDA calculations. A further molecular dynamics simulation allowed us to evaluate the phase diagram, reproducing correctly the non-trivial phase transition sequence of $BaTiO_3$. The structural parameters and coefficients of expansion are in very good agreement with experimental data, while the theoretically determined transition temperatures tend to be too small compared with experiment.

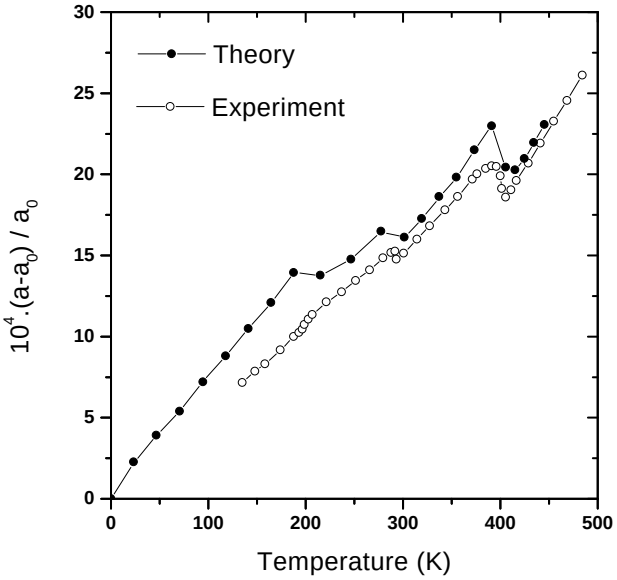

Figure 5. Comparison of experimental and MD results for the temperature dependence of the relative variation for the pseudocubic lattice parameter $a = V^{-1/3}$. V is the cell volume and a_0 is the value of a at 0 K. The abscissa and ordinate values for the model results have been rescaled (see the text).

Acknowledgments

This work was supported by Consejo Nacional de Investigaciones Científicas y Técnicas de la República Argentina. MGS also thanks Consejo de Investigaciones de la Universidad Nacional de Rosario and FONCyT for support.

References

[1] Cohen R and Krakauer H 1990 *Phys. Rev.* B **42** 6416
[2] Cohen R 1992 *Nature* **358** 136
[3] Resta R, Posternak M and Baldereschi A 1993 *Phys. Rev. Lett.* **70** 1010
[4] Ghosez P H, Gonze X and Michenaud J-P 1994 *Ferroelectrics* **153** 91
[5] Zhong W, King-Smith R D and Vanderbilt D 1994 *Phys. Rev. Lett.* **72** 3618
[6] Posternak M, Resta R and Baldereschi A 1994 *Phys. Rev.* B **50** 8911
[7] Singh D 1995 *Ferroelectrics* **164** 143
[8] Tinte S, Stachiotti M, Rodriguez C O, Novikov D L and Christensen N E 1998 *Phys. Rev.* B **58** 11 959
[9] Zhong W, Vanderbilt D and Rabe K 1994 *Phys. Rev. Lett.* **73** 1861
Zhong W, Vanderbilt D and Rabe K 1995 *Phys. Rev.* B **52** 6301
[10] Lewis G V and Catlow C R A 1985 *J. Phys. C: Solid State Phys.* **18** 1149
Lewis G V and Catlow C R A 1986 *J. Phys. Chem. Solids* **47** 89
[11] Donnerberg H and Bartram R 1996 *J. Phys.: Condens. Matter* **8** 1687
[12] Heifets E, Dorfman S, Fuks D and Kotomin E 1997 *Thin Solid Films* **269** 76
[13] Migoni R, Bilz H and Bäuerle D 1976 *Phys. Rev. Lett.* **37** 1155
[14] Perry C, Currat R, Buhay H, Migoni R, Stirling W and Axe J 1989 *Phys. Rev.* B **39** 8666
[15] Kugel G E, Fontana M D and Kress W 1987 *Phys. Rev.* B **35** 813
[16] Sepliarsky M, Stachiotti M and Migoni R 1995 *Phys. Rev.* B **52** 4044
Sepliarsky M, Stachiotti M and Migoni R 1997 *Phys. Rev.* B **56** 566

[17] Stachiotti M G, Sepliarsky M, Migoni R L and Rodriguez C O 1998 *First-Principles Calculations for Ferroelectrics (AIP Conf. Proc. No 436)* ed R E Cohen (Woodbury, NY: AIP) p 274
[18] Khatib D, Migoni R, Kugel G and Godefroy 1989 *J. Phys.: Condens. Matter* **1** 9811
[19] Blaha P, Schwarz K, Dufek P and Augustyn R 1997 *WIEN97* Technical University of Vienna
This is an improved and updated Unix version of the original copyrighted WIEN code, which was published by Blaha P, Schwarz K, Sorantin P and Trickey S B 1990 *Comput. Phys. Commun.* **59** 399
[20] Ceperley D M and Alder B J 1980 *Phys. Rev. Lett.* **45** 566
[21] Perdew J P and Zunger A 1981 *Phys. Rev.* B **23** 5048
[22] Kay H F and Vousden P 1949 *Phil. Mag.* **40** 1019
[23] Kwei G H, Lawson A C, Billinge S J L and Cheong S-W 1993 *J. Phys. Chem.* **97** 2368
[24] Ghosez P H, Gonze X and Michenaud J-P 1998 *Ferroelectrics* **206** 205
[25] Yu R and Krakauer H 1995 *Phys. Rev. Lett.* **74** 4067
[26] Nakamura T 1992 *Ferroelectrics* **137** 65
[27] Axe J D 1967 *Phys. Rev.* **157** 429
[28] Chen H and Callaway J 1992 *Phys. Rev.* B **45** 2085
[29] Lindam P J and Gillan M J 1993 *J. Phys.: Condens. Matter* **5** 1019
[30] Mitchell J P and Fincham D 1993 *J. Phys.: Condens. Matter* **5** 1031
[31] Mitsui T *et al* 1981 *Landolt–Börnstein New Series* Group III, vol 16 (Berlin: Springer)
[32] Shirane G and Takeda A 1952 *J. Phys. Soc. Japan* **7** 1